Multiscale characterization of pitting corrosion and application to an aluminum alloy

George N. Frantziskonis [a], Laura B. Simon [b], Jung Woo [c], Theodore E. Matikas [b]

[a] *University of Arizona, Department of Civil Engr. & Engr. Mechanics, Tucson, AZ 85721, USA*
[b] *University of Dayton, Center for Material Diagnostics, Dayton, OH 45469-0121, USA*
[c] *University of Arizona, Applied Mathematics, Tucson, AZ 85721, USA*

Abstract – This paper documents a novel method for characterizing pitting corrosion damage in structural materials such as Al 2024-T3. Specimens of such alloys are corroded in a controlled environment and the pits' geometry is captured digitally using white light interference microscopy. The digital data are then processed with wavelet-based analysis, thus making possible a multi-resolution description of the geometrical features. The analysis reveals several interesting features of the pits that are similar for all the experimental data analyzed herein, and independent of the process followed for creating them (time the material is exposed to corroding environment, concentration of the corroding agent, surface area exposed to the agent, etc.). The first property identified as common to all pits is their geometrical scaling with a (Hurst) exponent of 0.63 ± 0.12. Furthermore, the ratio ω of the surface area of the pit as represented at coarse scales through the wavelet representation, over the area of its intersection with the plane at zero depth is found to be 1.17 ± 0.07 consistently. The ratio of the total surface area over its intersection is found to be 1.6 ± 0.2. Either one of these ratios together with the Hurst exponent provide sufficient information for obtaining a pit's geometry from images capturing its two-dimensional shape only, a capability important for efficient characterization. Additionally, such a characterization is paramount for rigorously addressing fatigue crack initiation and propagation. © 2000 Éditions scientifiques et médicales Elsevier SAS

multiscaling / pitting corrosion / wavelets

1. Introduction

Environmental attack on structural materials is a problem directly related to the performance and integrity of structural components. A general review on this subject is not attempted herein, yet reference is given to those works directly related to this study which focuses on pitting corrosion damage, commonly observed in a wide range of aluminum and steel alloys, and recognized as the main fatigue crack nucleation site (Piascik and Willard, 1994; Chen et al., 1996; Ahn et al., 1992); from these references the rather extensive literature on the subject can be traced. Although significant research has been performed on the effects of defects on structural fatigue life, a quantitative method which assesses the role of corrosion damage on fatigue behavior (nucleation and propagation) is presently under investigation by several research groups. Such a method, as can be reasoned on physical grounds, would rely heavily on efficient characterization of pitting corrosion. Thus, there is a need for robust characterization as well as for acquiring pitting corrosion data in an efficient manner, and this work addresses both of these issues.

In particular, this work attempts to characterize corrosion pitting damage through multiscale analysis and identify: (a) properties that allow complete characterization from two-dimensional images of pitting, which are easily acquired in practice; (b) the morphology of the pits, described in a multiscale fashion, important for crack initiation and propagation under fatigue loading.

1.1. *Wavelet analysis*

Wavelet analysis is being used to rationalize information at various scales in several branches of science, including particle physics, biology, electrical engineering, fluid mechanics, and medicine. However, this powerful technique has not been applied to characterize degradation of materials, e.g., corrosion, even though many critical questions could be addressed.

The wavelet transform can be seen as a mathematical microscope: when increasing the magnification, one gains insight into the intricate structure of a 'pattern'. Wavelets provide a means to mathematically represent functions space- and scale-wise with a few parameters. The so-called wavelet coefficients provide local information on the function and also information relevant to scale (level of magnification). Fourier transforms, based on combinations of sines and cosines, are very useful for describing periodic and stationary functions, but they are not useful for the many nonperiodic, nonstationary phenomena encountered in the physical world. Hence, the use of wavelets has found riches in analyzing complex signals and structures, e.g., in turbulence, but heretofore wavelets have not been used as a tool in analyzing corrosion 'structures'.

Notable advances in applications of wavelet methods have increased tremendously in the past few years (Meyer, 1991; Daubechies, 1992; Ruskai et al., 1992; Meyer and Roques, 1993; Benedetto and Frazier, 1994; Newland, 1994; Chui et al., 1992–1997; Frantziskonis and Loret, 1995; Szu, 1996; Aldroubi and Inser, 1996; Andreas and Trevino, 1997; Kumar and Foufoula-Georgiou, 1997). A paradigmatic illustration is material microstructure where the hierarchy of initial and induced heterogeneity prohibits its rational description independently of scale. Due to the capability of wavelet analysis to rationalize data in both scale and space simultaneously, we can analyze the existence of structures and patterns for which no other technique is adequate.

The remaining of this subsection provides a review of some of the important mathematical properties of wavelets, without any attempt at being complete. The aim is to provide background adequate for the following sections.

The wavelet transform is an integral transform developed in the eighties in signal analysis and is today used in different fields as mentioned before. The wavelet transform behaves as a mathematical microscope, which decomposes an input signal or image into amplitudes which depend on position and scale. For this purpose localized functions, called wavelets, are being used. By changing the scale of the wavelet, one is able at a certain location to focus on details at higher and higher resolution. Here we mention some of the important properties of wavelets. For a more complete treatment of wavelet analysis see, e.g., (Daubechies, 1992).

In science and engineering there are many problems more easily solved in a new set of coordinates (basis), the Fourier transform being one. Using such transforms one calculates the amplitudes for each basis function in the new domain. The wavelet transform is an attractive and rather new (integral) transform, the attractiveness being that the set of basis functions (wavelets) are chosen to be well-localized (have compact support) both in space and frequency. Thus, one has a dual-localization of the basis functions. This contrasts the situation met for the Fourier transform where one only has mono-localization, i.e., localization in both position and frequency simultaneously is not possible. A remarkable feature of the wavelet transform is that the basis is constructed from a single function $\psi(x)$, the so-called 'mother' wavelet, i.e.,

$$\psi_{a,b}(x) = \psi\left(\frac{x-b}{a}\right), \tag{1}$$

where $a > 0$ is a scale parameter and $-\infty < b < \infty$ is a translation parameter. For a function $f(x)$ (generalization to functions in higher dimensions is straightforward) the wavelet transform is

$$W[f](a, b) = \frac{1}{\sqrt{a}} \int_{-\infty}^{\infty} f(x)\psi_{a,b}(x) \, dx. \tag{2}$$

Wavelet functions used as analyzing wavelets must have zero mean, and in most applications it is imperative that are orthogonal to some lower order polynomials, i.e.,

$$\int_{-\infty}^{\infty} x^m \psi(x) \, dx = 0, \quad 0 \leqslant m \leqslant n, \tag{3}$$

and the maximum vanishing moment, integer n, is directly related to the so-called order of the wavelet. The vanishing moments are important, especially for problems with a 'drift' as will be addressed later.

2. Experimental program and results

Standard dog-bone samples [E-466-96-ASTM] (*figure 1*), were fabricated from high strength, aerospace aluminum alloy 2024-T3. The chemical composition (in wt. %) of this alloy is 4.60 Cu, 1.53 Mg, 0.63 Mn, 0.19 Fe, 0.13 Zn and the rest Al. The ultimate tensile strength is 490 MPa and the yielding stress 350 MPa. The material was purchased as one flat bare sheet and the dog-bone samples were cut having the tensile axis in the rolling direction. Pits were created on the fatigue dog-bone samples using the following procedure (Simon et al., 1998).

Initially, the samples were polished with 600 grit SiC, rinsed with distilled water and dried in a stream of air. In order to control the number of pits, all but a 10 mm^2 area in the center portion of the sample was covered with a green waterproof sealing tape, as shown in *figure 1*. In later experiments, this exposed surface was coated with a clear fingernail polish. After a few minutes, when the polish became tacky, 2–3 fine holes were introduced into the polish using the tip of a needle. The sample was then placed in an electrochemical cell and anodically polarized to create corrosion pits. The electrolyte used was 0.1 M NaCl. The counter electrode was a Pt mesh screen, and a saturated Calomel electrode served as the reference electrode.

After experimenting with various polarization techniques, a potentiostatic scan was developed to produce the best controlled pitting condition. This polarization scheme involves setting the potential at a predetermined
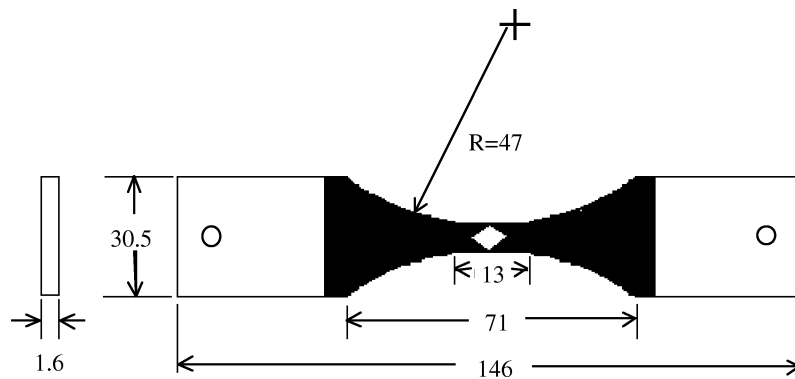

Figure 1. Standard fatigue dog-bone sample covered with waterproof tape. Dimensions are in millimeters.
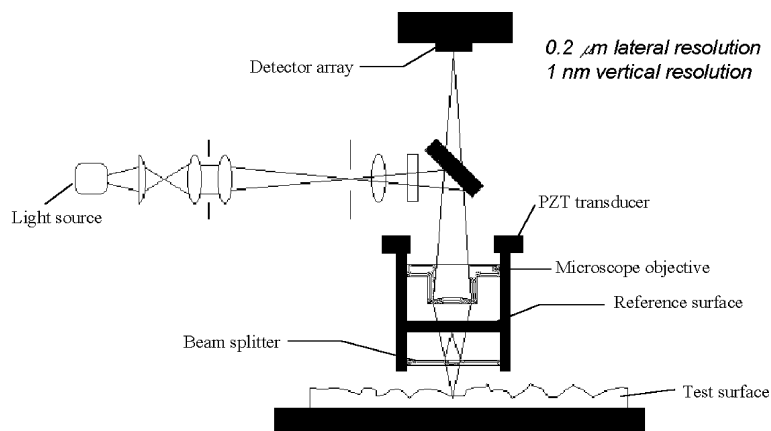
Figure 2. Schematic of white light interference microscope.

fixed value. The current is then monitored as a function of time. The sample had to be polarized several times in order to produce 2–3 large, deep pits. The potential is initially set at about –500 mV vs. SCE, and then dropped to around 550 mV to –600 mV vs. SCE for the remainder of the anodic polarizations. In general, it took 24–48 h to create pits for each sample. The total polarization time ranged from 11–25 h depending on the sample. This produced relatively large pits having depths between 50 and 200 μm.

After the sample was polarized, a surface profile of the pitted samples was obtained using white light interference microscopy. Advantages in using this instrument include fast imaging with high resolution. The lateral resolution of the equipment is 0.2 μm, and the vertical 1 nm. A schematic of the white light interference microscope is shown in *figure 2*. Vertical scanning-interferometry (VSI) was used for these aluminum samples. This technique utilizes an unfiltered white light beam which passes through a microscope objective to the sample surface. A beam splitter is provided to reflect half of the incident beam to the reference surface. At the beam splitter, the white light is then reflected from the reference mirror and combines with the light reflected from the sample surface to produce interference fringes, and the highest contrast fringe provides the best focus. The system measures the degree of fringe modulation or coherence. During an actual measurement, the reference arm holding the interferometric objective has the capability to automatically move in a vertical direction to scan the surface at varying heights. A linearized piezoelectric transducer precisely controls this motion.

Figure 3a shows a typical three-dimensional plot of a pit produced and digitized by the processes described previously. *Figure 3b* shows a cross-section of the pit. Several pits were digitized and used for the subsequent analysis. *Figure 4* shows some typical cross-sections from pits corroded for a variety of times. Apparently, there is no 'trend' in the shape or the depth of each corroded volume.

3. Wavelet analysis of corroded surfaces

The first step in the analysis is to see whether there is any statistical 'similarity' among all corroded surfaces. It has been known for quite some time that self-affine surfaces are abundant in nature. They can be found in various areas of science, such as surface growth (Meakin, 1993; Barabasi and Stanley, 1995) fracture surfaces (Bouchaud et al., 1990), biological systems (Vicsek et al, 1990), and even in stock market (Bak and Paczuski, 1995). In a recent work (Simon et al., 1998) a very efficient method for determination of the Hurst exponent (for self-affine surfaces) was introduced and examined in detail. The method, based on wavelet analysis of data,
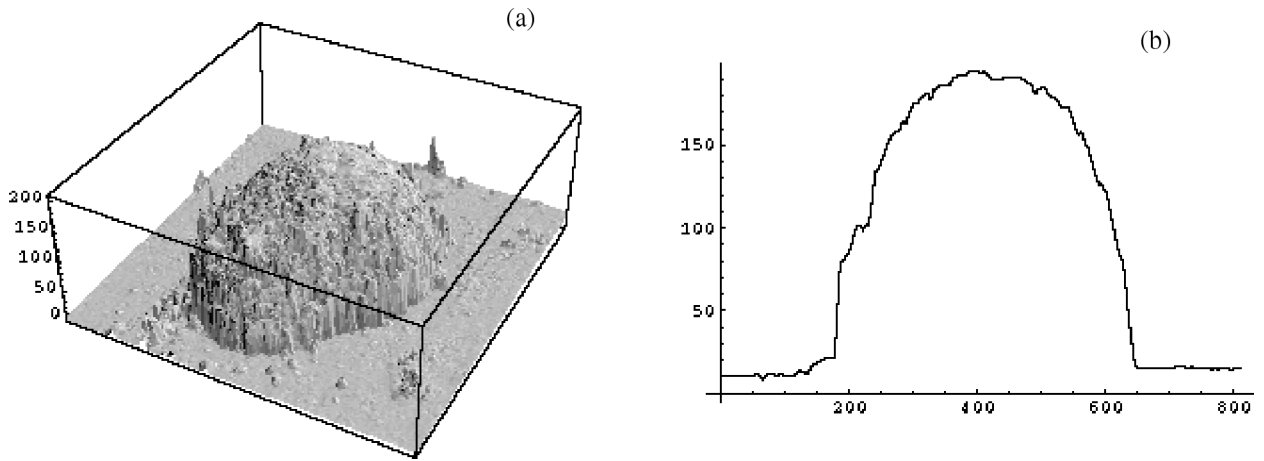
Figure 3. (a) Three-dimensional view of a corrosion pit. For clarity it is shown as a 'mountain' rather than as a 'pit'. The horizontal dimensions are 809 μm × 809 μm digitized into a 256 × 256 pixels grid and the vertical axis is in μm. The maximum height (depth) is 203.82 μm. The sample was corroded for 11 h. (b) A cross-section of the pit shown in (a); both axes are in μm.

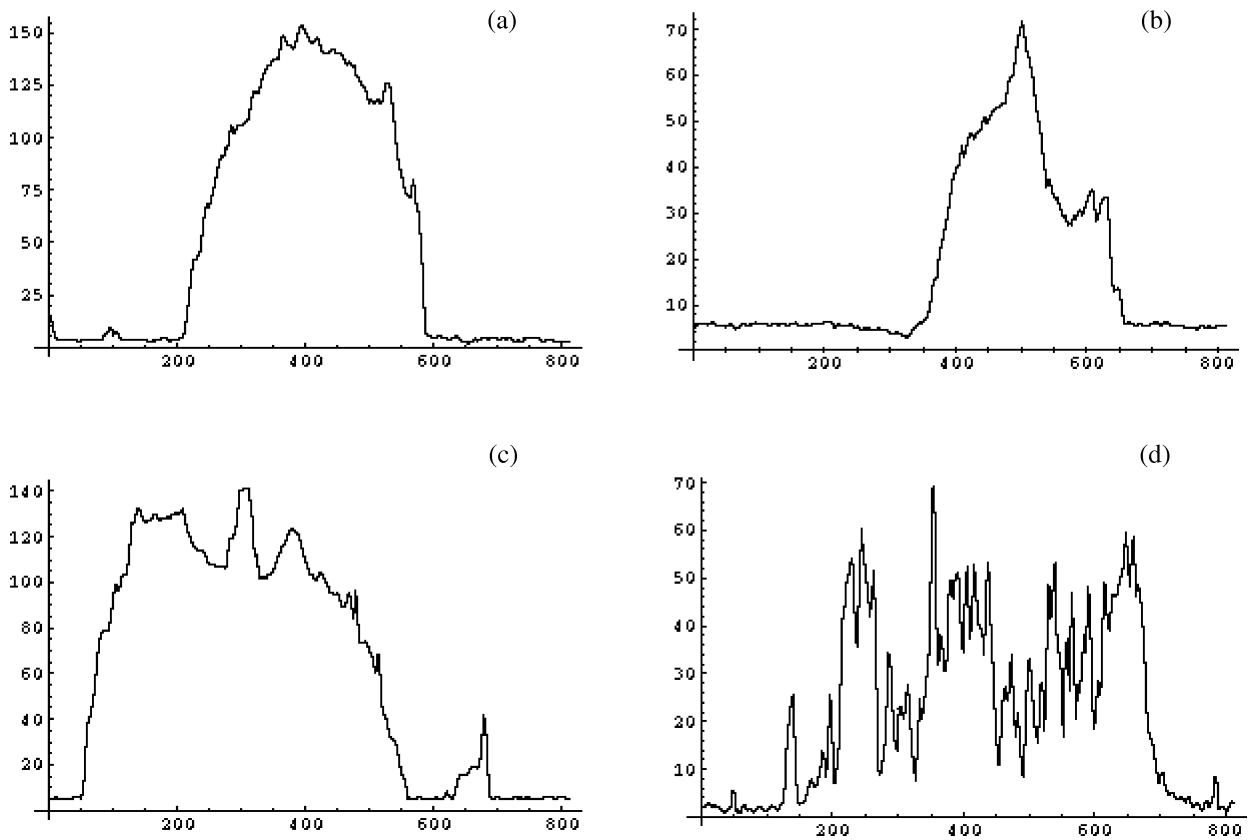**Figure 4.** Four sections from four different pits. (a) from one corroded for 11 h; (b) 4.38 h; (c) 17.65 h; (d) 22.5 h. All axes are in μm.
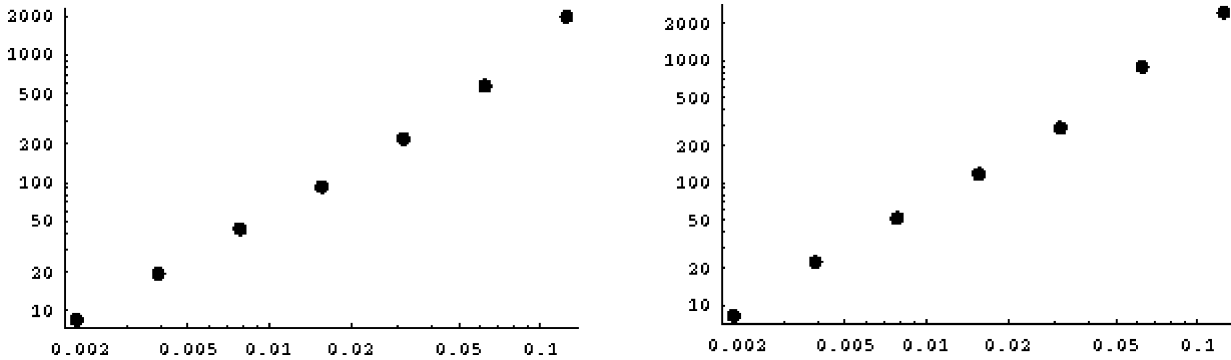
Figure 5. Typical log-log plots of a, horizontal axis, versus M_a. (a) from the pit shown in *figure 1*, horizontal direction; (b) vertical direction.

is clearly shown to outperform other methods available, especially when a small number of samples, or even single realizations are available. As shown when a function $f(x)$ scales, in a statistical sense, such that

$$f(x) = \lambda^{-H} f(\lambda x) \tag{4}$$

then its wavelet transform satisfies

$$W[f](\lambda a, \lambda b) = \lambda^{H+1/2} W[f](a, b). \tag{5}$$

By averaging out the dependency on the translation parameter b, i.e., by calculating, for each scale of decomposition a

$$M_a = \left\langle \left| W[f](a, b) \right| \right\rangle_b \tag{6}$$

and by plotting, in log-log plot, a versus M_a, the slope of the straight line (for self-affine surfaces) is $1/2 + H$. Of course, since data in this case (pit geometry) are two-dimensional, we choose to examine two perpendicular directions, i.e., x and y. Different H in the two directions implies anisotropy. The results shown in the following were obtained using the so-called Daubechies family of wavelets (Daubechies, 1992). Unless otherwise indicated the wavelet used is the Daubechies wavelet with four vanishing moments.

Figure 5 shows two typical log-log plots of a versus M_a; for compactness only typical log-log plots are provided herein, and instead slopes (H) from several pits are provided in *figure 6*. As would be expected from the way the pits were created, no anisotropy trend could be identified.

On a 'strict' statistical basis, the number of surfaces examined is not large enough for making definite conclusions on scaling properties, yet a trend towards $H \cong 0.63$ can be identified. This is important for two reasons. First, by knowing H, the statistical properties of horizontal cross-sections, and thus of the intersection with the metal surface, are known (Alexander, 1986), i.e., each cross-section is self-similar with a fractal dimension $D = 1 - H$. This, together with the properties addressed in the following section provides adequate information for identifying the 3-D morphology of a pit from 2-D images. While white light interferometry is very efficient in capturing the 3-D geometry of pits, it is mostly used in laboratories since, similarly to most techniques capable of providing 3-D images of surfaces, its use in the field is very inconvenient and expensive (e.g., for capturing the morphology of a large number of pits). To the contrary, 2-D images of pitting are easily acquired in practice. Second, the roughness characteristics of the surface at micro-scales should be known if one wishes to develop techniques predictive of crack initiation and propagation under fatigue loading (such techniques are outside the central theme of the present work).
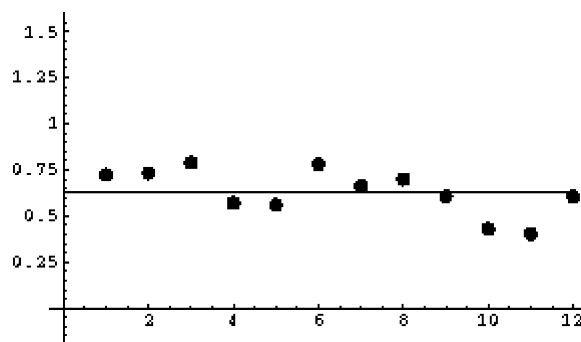
Figure 6. Values of H (vertical axis) for six different pits. For each pit the H in two transverse horizontal directions is shown. The value of H, from that data is 0.63 ± 0.12 (confidence level 95 %).

The previous analysis examined the roughness of the surfaces, and any drift was not included in the analysis. Based on the 'appearance' of the surfaces (*figures 3* and *4*), one would expect a drift. Because of the vanishing moments of wavelets, equation (3), polynomials (drift) of degree less or equal to n are automatically removed from the surface analysis. We used wavelets with four vanishing moments. With this, it can be comfortably stated that the roughness study above removed drift, especially for fine scales (Simon et al., 1998). In order to study the drift, several properties of the pits can be studied. It is interesting that the wavelet representation of a function at very coarse scales, i.e., the representation through the scaling function, provides the 'trend' or the drift in our case. For example, *figure 7* shows the drift of the curve shown in *figure 3b* as obtained by the representation of the curve at very coarse scales, i.e. through the scaling function.

Several measures of the pits were examined, especially with respect to the time the material was exposed to a corrosive environment. Yet, it is found that the ratio ω of the surface area of the pit represented at coarse scales over the area of its intersection with the plane at zero depth is 1.17 ± 0.07 (confidence level of 95 %), while the ratio of the total pit area (measured at the finest resolution, i.e., the resolution used in capturing the pits' geometry, over the intersection is 1.6 ± 0.2 (confidence level of 95 %). Perhaps this has a chemistry-based explanation, even though the trend of the pit is involved in this ratio. It may be appropriate at this point to comment that it is known that invasive fractality of many treated metal surfaces is responsible for improving the absorption properties of the boundary. Therefore, corrosion agents, as is the case relevant to this work, behave in a peculiar manner on fractal surfaces, depending on their particular energy-absorption properties; we refer to (Carpinteri et al., 1997) and (Le Méhauté, 1991) and references cited therein for interesting topics relevant to this; it is outside the central theme of the present paper thus further details are not provided herein.

Based on the above analysis, the strategy for obtaining information on the 3-D morphology of a pit from 2-D images (transverse to the material surface) is as follows: (1) From the 2-D data obtain the trend (perimeter) of the intersection of the pit with the material surface; since the 2-D data are either from optical microscopy or SEM any 'noise' in the image, e.g., from features other than the pit, should be removed from the image. Note that the wavelet transform of the 2-D image can also be used for extracting the perimeter of the pit. (2) Measure the total area of the 2-D pit, and using ω estimate the 3-D pit's total surface area. (3) Using interpolation functions, construct the three-dimensional trend such that the ratio ω is ~ 1.17. A non-systematic study has shown that using, for each point, its minimum distance from the perimeter as its 'depth' provides a good interpolation scheme; then by increasing those depths proportionally until the proper ω is achieved we obtain the pit's trend. (4) On the constructed 3-D trend superimpose a self-affine surface with $H \sim 0.63$.
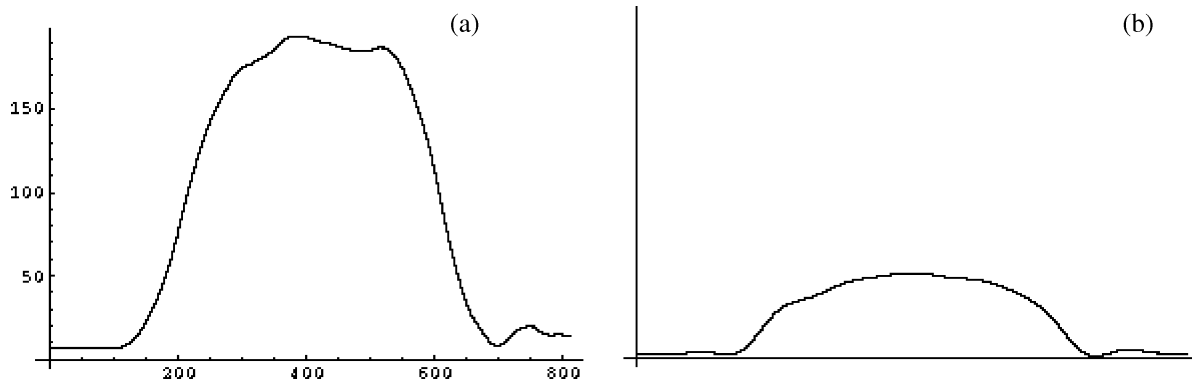
Figure 7. (a) the representation of the curve of *figure 3b* at coarse scales; both axes are in μm. (b) the same as (a) with both axes scaled identically; this indicates that the pits are wide and 'shallow'.
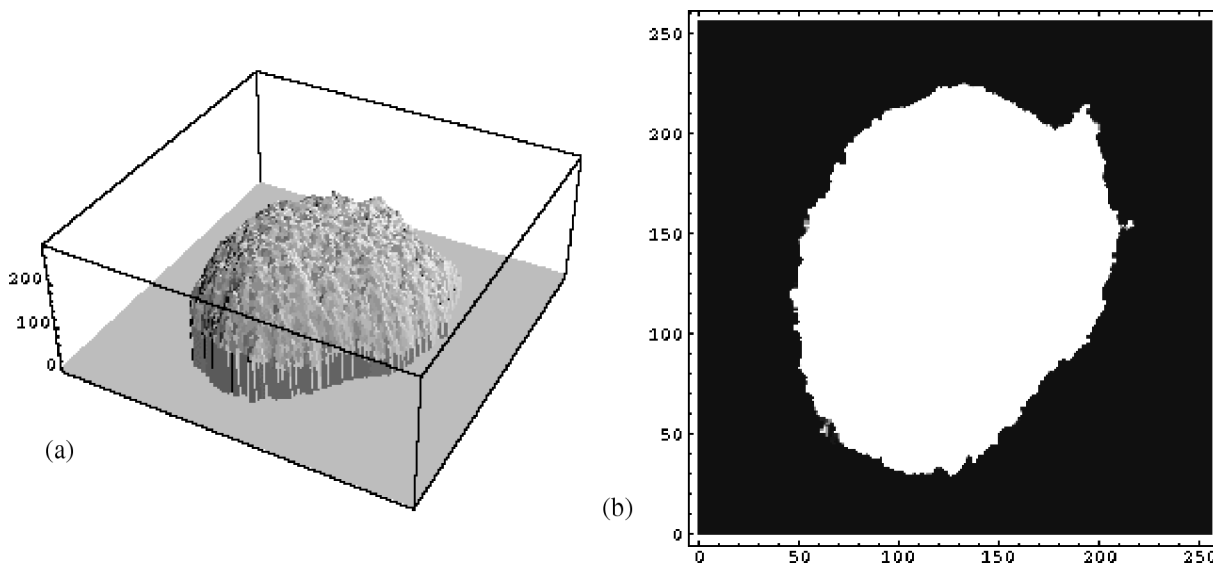

Figure 8. (a) The 3-D geometry of the pit shown in *figure 3*, as reconstructed using WRM. The vertical axis is in μm. The image of (b), which is the pits 2-D geometry as obtained from optical microscopy (after minimum processing to 'homogenize' the area inside and outside the pit) was used for the reconstruction.

We call this simple method the Wavelet Reconstruction Method (WRM). *Figure 8a* shows the pit as reconstructed using the WRM from an optical microscope image of the pit. For comparison, the pit's geometry (obtained using profilometry) is shown in *figure 3*.

As can be seen, the method reconstructs the pit's 3-D geometry reasonably. Note that the WRT is statistical, so its capability to reconstruct the images is evaluated for the ensemble average rather than for individual realizations. Thus, for example, the two images in *figure 9* are statistically close to one another (this is partially indicated in a table shown in the sequence). Yet, the method cannot foresee any 'special' features in the geometry, as shown, for example in *figure 9*. Here, the pit shows a non-uniform depth, e.g., depth is higher at the left of *figure 9a*. This, as expected, is not captured by WRM 'exactly', but rather, statistically. Yet, as shown in the sequence, several properties of pits are captured reliably.
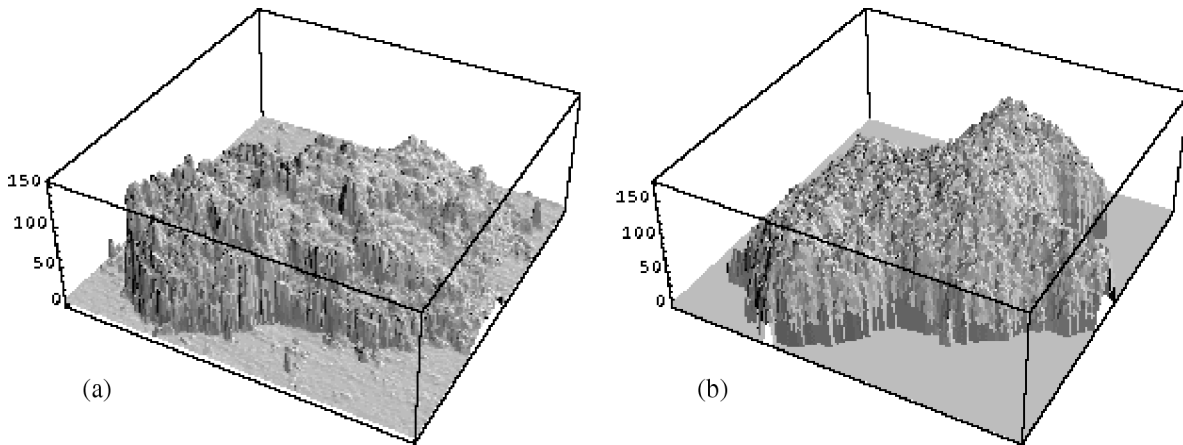
(a)   (b)

Figure 9. (a) A pit captured using profilometry; (b) The same pit as reconstructed from 2-D SEM microscopy, using the WRM.

Table I.

Test Series	L	H	L	K
Corrosion time	11 h	17.6 h	11 h	4.38 h
Volume from profilometry (μm^3)	2.91818×10^7	2.98312×10^7	1.9544×10^7	0.69867×10^7
Volume based on optical images or SEM (μm^3) – evaluated through WRM	2.87617×10^7	3.26622×10^7	2.15657×10^7	1.48768×10^7
Max. pit depth from profilometry (μm)	203	151	173	97
Max. pit depth based on optical images or SEM (μm) – evaluated through WRM	223	151	198	125
Surface area from profilometry (μm^2)	452×10^3	551×10^3	355×10^3	219×10^3
Surface area based on optical images or SEM (μm^2) – evaluated through WRM	392×10^3	378×10^3	316×10^3	225×10^3

Table I shows four test results examined with WRM. The 'test series' implies the specimen on which the pits were created. The pits' perimeter was extracted from optical microscopy or SEM as indicated. As can be seen, the technique is reliable in providing important geometrical pit properties.

4. Discussion and conclusions

The wavelet analysis allows a multiscale description of the morphology of corrosion pitting, and it has been clearly shown that obtaining 3-D information from 2-D images is achievable. Additionally, the process is rather independent of the magnification the 2-D pitting images are captured in; within a range of magnifications, of course, as far as the perimeter of the pit is captured in enough detail. The work is amenable to examining a large number of corroded surfaces, corroded under various conditions, by obtaining both 3-D and 2-D images at a range of magnifications.

Using profilometry, sharp vertical 'jumps' of a surface may indicate either an actual vertical jump, or a hidden 'overhang' in a pit's morphology. The experiments so far do not show such sharp vertical jumps; yet this does not imply all pits do not have them. Thus, the present technique is amenable to cross-correlation with other techniques capable of capturing the geometry of pits.

The multiscale information present in a pit's morphology 'prohibits' the study of crack initiation and propagation using traditional techniques. For example, one even has to address the problem of stress concentration in a multiscale fashion. Having a multiscale description of the morphology readily available, the following tasks are applicable here: examination of the implications of a multiscale morphology on the stress analysis of a structure (specimen), e.g., stress concentrations, intensity factors (when definable), etc.; examination of the implications of a multiscale morphology on the microstructural changes going on during fatigue loading. This part is now being examined nondestructively, numerically and analytically. In short, we believe the present multiscale approach paves the way towards new avenues in pitting corrosion characterization and implications to structures.

Acknowledgements

References

Ahn S.H., Lawrence F.V., Jr., Metzger N.M., 1992. Corrosion fatigue of an HSLA steel. Fatigue Fract. Engrg. Mater. Struct. 15, 625–642.

Aldroubi A., Inser M. (Eds.), 1996. Wavelets in Medicine and Biology. CRC Press Inc., Boca Raton, Florida.

Alexander S., 1986. In: Klafter J.R. et al. (Eds.), Transport and Relaxation in Random Materials. World Scientific, Singapore.

Andreas E., Trevino B., 1997. Using wavelets to predict trends. J. Atmos. Ocean Tech. 14 (3), 554–564.

Bak P., Paczuski M., 1995. Complexity, contingency, and criticality. Proc. Nat. Acad. Sci. 92, 6689–6694.

Barabasi L., Stanley H.E., 1995. Fractal Growth Models. Cambridge University Press, Cambridge.

Benedetto J.J., Frazier M.W. (Eds.), 1994. Wavelets, Mathematics and Applications. CRC Press, Boca Raton, Florida.

Bouchaud E., Lapasset G., Planes, 1990. Fractal dimension of fractured surfaces: A universal value? J. Europhys. Lett. 13, 73–78.

Carpinteri A., Chiaia B., Nemati K.M., 1997. Complex fracture energy dissipation in concrete under different loading conditions. Mechanics of Materials 26, 93–108.

Chen G.S., Wan K.C., Gao M., Wei R.P., Flournoy, 1996. Transition from pitting to fatigue crack growth–modeling of corrosion fatigue crack nucleation in a 2024-T3 aluminum alloy. Matl. Sci. Engrg. A 219, 126–132.

Chui C.K. et al., 1992–1997. An Introduction to Wavelets, Vols. 1–6, Academic Press, San Diego.

Daubechies I., 1992. Ten Lectures on Wavelets. SIAM, Philadelphia.

Frantziskonis G., Loret B., 1995. Scale dependent constitutive relations – information from wavelet analysis and application to localization problems. Eur. J. Mechanics A/Solids 6, 873–892.

Kumar P., Foufoula-Georgiou E., 1997. Wavelet analysis for geophysical applications. Review of Geophysics 35 (4), 385–412.

Le Méhauté A., 1991. Fractal Geometries: Theory and Applications. CRC Press, Boca Raton, Florida.

Meakin P., 1993. The growth of rough surfaces and interfaces. Phys. Rep. 235, 189.

Meyer Y. (Ed.), 1991. Wavelets and Applications. Masson, Springer-Verlag, Paris.

Meyer Y., Roques S. (Eds.), 1993. Wavelet analysis and Applications. Editions Frontieres, Singapore.

Newland A., 1994. Wavelet Analysis of vibration, Part 1, 2. Trans. of the ASME, J. of Vibration and Acoustics 116 (4), 409–425.

Piascik R.S., Willard S.A., 1994. The growth of small corrosion fatigue cracks in alloy 2024. Fatigue Fract. Eng. Mater. Struct. 17, 1247–1260.

Ruskai M.B. et al. (Eds.), 1992. Wavelets and Their Applications. Jones and Bartlett Publ., Boston.

Simon L.B., Khobaib M., Matikas T.E., Jeffcoate C.S., Donley M.S., 1998. Controlled pitting in aluminum 2024-T3 alloy. Corrosion, to appear.

Simonsen I., Hansen A., Nes O.M., 1998. Determination of the Hurst exponent by use of wavelet transform. Phys. Rev. E 58 (3) 2779–2787.

Szu H.H. (Ed.), 1996. Wavelet Applications III. Proceedings of SPIE, Vol. 2762.

Vicsek T., Cserzo M., Horvath V.K., 1990. Self-affine growth of bacterial colonies. Physica A 167, 315–394.